Technical Data Package for the ESS Critical Design Review of the Raster Scanning Magnet System

H.D. Thomsen,* S.P. Møller

Department of Physics and Astronomy, Aarhus University (AU)
8000 Aarhus C, Denmark

September 24, 2015

Abstract

This note is to serve as a central document that combines several supporting technical documents into a data package for the European Spallation Source (ESS) Critical Design Review (CDR) of the Raster Scanning Magnet (RSM) system located in the Accelerator to Target (A2T) region. It should be stressed that the note covers only the RSM system and not the remaining parts of Work Package 6 (WP6) unless strong links are present.

This note is to provide executive summaries of the documents that cover the topics of the CDR charge. In several cases, this document will provide further details or comment on recent changes that have been introduced since the completion of the supporting documents.

---
*heinetho@phys.au.dk

Contents

1 Introduction

The raster system generates pulsed triangular magnetic field waveforms acting in both the horizontal (H) and vertical (V) direction with 4 magnets acting in each direction. By maintaining a H-V waveform frequency ratio differing from unity, the proton beam centroid follows a Lissajous-like displacement pattern on the target during the raster pulse. Although the design of the RSM magnet and supply has officially been developed by Aarhus University (AU) from the very beginning, it should however be stressed that the initial feasibility and design studies were only possible due to the friendly and eager support from highly skilled and experienced collaborators at ESS, CERN, and elsewhere. AU only has limited expertise within pulsed magnet and supply design at hand, hence a technical design study of the system, including *e.g.* circuit simulations, of the system was subcontracted to a local supplier of accelerator components, Danfysik, and completed in 2014 [1]. Due to the lack of local expertise and resources, the RSM project is to proceed by an open call for tenders with a contract that will include the responsibility for the final magnetic, electrical, mechanical and thermal design of the magnets and power supplies, their construction, followed by their magnetic, mechanical, electrical, thermal, reliability testing, and finally delivery to AU or ESS. The product consists of a pulsed RSM system that is complete in the sense that all necessary magnets, power supplies, cables, ceramic vacuum chambers, system performance monitors, support stands, and local control systems are included in the procurement. Only few qualified suppliers are available in the field of novel turn-key pulsed magnet systems. We are convinced that several of these will not accept the design and pre-series project at a reasonable price level without being guaranteed the production of the full production series.

The first delivery will be a 2-magnet pre-series that will undergo long-term performance and reliability testing at AU (Site Acceptance Test I, cf. Sec. 7). If the pre-series is found acceptable, the full 8-magnet production series will be initiated, possibly with minor alterations based on the experience with the pre-series.

1.1 Definition of Project Phases

1. Phase I (design phase) will consist of the following milestones:

    - Magnetic field calculations by the Supplier
    - Power supply and cable design and simulations by the Supplier
    - Detailed design report by the Supplier
    - Factory Acceptance Test I & II proposal by the Supplier
    - Acceptance of the detailed design of the Product by AU
    - Acceptance of the Supplier's proposal for the tasks to be completed during Factory Acceptance Test I by AU
    - Factory Acceptance Test I

2. Phase II (pre-series manufacture) will consist of the following milestones:

    - Production and assembly of parts by the Supplier
    - Implementation of local control system by the Supplier
    - Factory Acceptance Test I by the Supplier and approval by AU
    - Delivery to AU (Site I) by the Supplier

- Installation and assembly of the Pre-series Product by the Supplier

3. Phase III (Pre-series long-term testing at Site I) will consist of the following milestones:

   - Site Acceptance Test I by AU
   - Magnetic and stability testing by AU
   - Factory Acceptance Test II by the Supplier and approval by AU
   - Pre-series Performance Acceptance Test

4. Phase IV (Production-series manufacture) will consist of the following milestones:

   - Production and assembly of parts for the Production-series Product by the Supplier
   - Factory Acceptance Test II by the Supplier and approval by AU
   - Delivery to Site II by the Supplier

5. Phase V (Site Acceptance Test II) will consist of the following milestones:

   - Site Acceptance Test II
   - Site Approval

The schedule for the project phases can be inspected in Section 3 of [2]. The schedule is to be reviewed, once a supplier is selected. Before each design or equipment acceptance milestone is completed, we expect that AU will produce reports containing clear suggestions on how to proceed. ESS is to review the suggestions before the supplier is allowed to proceed. Depending on the complexity of the acceptance milestone, the consent should follow from either brief communication with designated supervisors or minor panel reviews.

1.2 Supporting Documents and Material

In the following a number of technical notes, drawings and other material will be referenced. Additionally, the material for the pending open call for tenders is included in the current state of the documents:

- Instructions to Tenderers (ITT) [2].
- Contract [3].
- Appendix 1: Technical Specifications [4].

In particular, the reader's attention is directed to [4], which contains the technical specifications as they will be communicated to potential suppliers.

2 Requirements

During the A2T Internal Vertical Design Review (IVDR) the L3 and L4 technical and interface requirements of the RSM system were discussed and agreed upon. We believe that the current RSM system design is consistent with L2–L4 requirements.

Table 1: Beam parameters, horizontal (H) and vertical (V), at the Crossover, PBW, and BEW.

| Parameter	Unit	Location	H	V
RMS beam size	mm	Crossover	0.14	0.64
	mm	PBW	10.7	4.10
	mm	BEW	13.5	5.05
Max. displacement	mm	PBW	47.1	15.8
(rastering)	mm	BEW	59.5	20.0
n_w	—	—	113	83
f_w	kHz	—	39.55	29.05
Avg. current density	$\mu A/cm^2$	PBW	84	
	$\mu A/cm^2$	BEW	53	
Footprint: 99.0%	mm	BEW	160	60
99.9%	mm	BEW	180	64

3 BDS Optics Design

3.1 Introduction

The beam optics of the A2T region is determined by the setting of DC quadrupole magnets and AC raster scanning magnets. A set of 8 dithering RSM dipoles, 4 acting in each plane, introduces fast AC transverse beam centroid displacements at the target and Proton Beam Window (PBW). Setting a sweep frequency ratio in the two planes, f_x/f_y, the RSMs produce a fine-meshed Lissajous-like, diagonal crosshatch pattern with an rectangular outline, cf. Fig. 1a. Such an approach, combined with a $\simeq 0.68$ cm^2 beamlet, generates a time-averaged intensity distribution with a large uniform central region and less than 1% beam deposited outside the 160×60 mm^2 nominal footprint. Beamlet sizes and displacement amplitudes at the location of the PBW and the target surface, the Beam Entrance Window (BEW), can be seen in Table 1. A frequency ratio of $f_x/f_y = 113/83$ (possibly $f_x = 40$ kHz and $f_y = 29$ kHz) has been assumed for the simulation, and the resulting time-averaged intensity distribution can be inspected in Fig. 1b. The nominal beam optics principles and conditions of the beam delivery systems and the RSM system is described in detail in several reports, *e.g.* [5].

3.2 Error & Tolerance Studies

The robustness of the nominal DC optics lattice has been probed by injecting a wide range of typical error sources that affects the beam dynamics [6]. The errors sources are classified into two different kinds: dynamic (fast) and static (slow). The dynamic errors have an origin or change on a timescale that generally prevents feasible correction schemes. This could be magnet support vibrations (displacements) or ripple from the magnet power supply.

The error types and magnitudes can be seen in Table 2. These are implemented in TraceWin [7], which is used for the simulations. Included are magnet transverse displace-
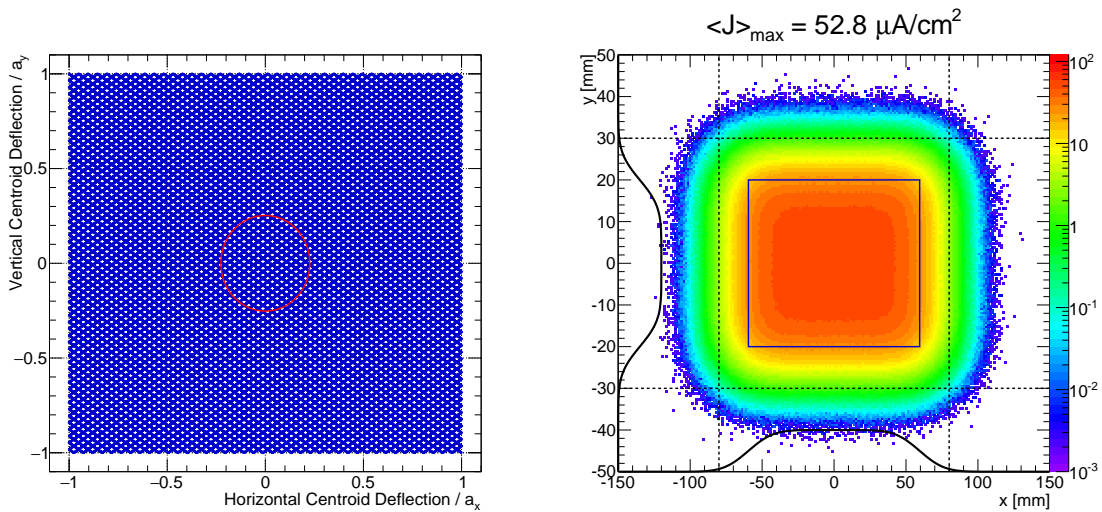
(a) A Lissajous-pattern generated by triangle waveforms with a frequency ratio of 113/83. For comparison, the beamlet relative RMS sizes at the BEW are illustrated by a red ellipse.

(b) The intensity distribution is scaled to represent the peak current density, normalized to 2.5 mA average current. The blue rectangle illustrates the outline of the raster pattern. The dashed lines indicate the footprint containing 99.0% of the beam. Notice the 3:1 aspect ratio on the scales.

Figure 1: Simulated raster pattern and consequent intensity distribution at the target BEW following a full cycle of the Lissajous-pattern with the beam parameters in Table 1.

ment (dx, dy), roll $d\hat{z}$, and strength offset. The two dogleg dipoles are powered by a single power supply, hence the dipole strength errors are introduced as a coupled error. All other errors are treated as uncoupled. Besides phase space displacements (dx, dx', dy, dy'), the High Energy Beam Transport (HEBT) input beam is exposed to energy jitter, emittance and current increase. A mismatch factor m_w also affects the Twiss parameters, $(\alpha_w, \beta_w) \rightarrow (1 + m_w) \times (\alpha_w, \beta_w)$ in each plane $w = x, y, z$. The magnitudes of the errors have been set by looking at similar single-pass lines but also by consulting experienced magnet designers for comments on feasibility and pricing. For reference the RMS beam size is $\simeq 2$ mm at the interface between the High-Beta linac and the HEBT.

3.2.1 Multiparticle Studies

Combining all of the above, an error study based on multiparticle simulations has been performed [6]. Specifically, the envelope optics are used to apply dynamic and static errors and correct the latter using a range of virtual diagnostics. For each of 1000 simulated HEBTs, the achieved optics is then the basis of a multiparticle simulation with 10^6 macroparticles. The applied input beam distribution consists of two overlapping Gaussians: a primary (99%) Gaussian distribution and a secondary (1%), with $5\times$ emittance, representing beam halo. The simulated HEBTs have been combined and are represented in Fig. 2 by contour lines that transversely enclose beam power levels. The contours are to a large extent comparable to the 10 RMS nominal beam size envelope (blue line). Due to the uncorrected input beam mismatch, some beta-beating is visible in the first 200 m. This is also believed to be the cause of an observed increase in transverse emittance, typically 10%, max. 20%, within the first 50 m of the HEBT. This could be reduced by applying the corrective matching in the beginning of the HEBT.

6

Table 2: Definition of error types and magnitudes. Unless otherwise specified, the values represent the half-width of a uniform distribution centered around 0.

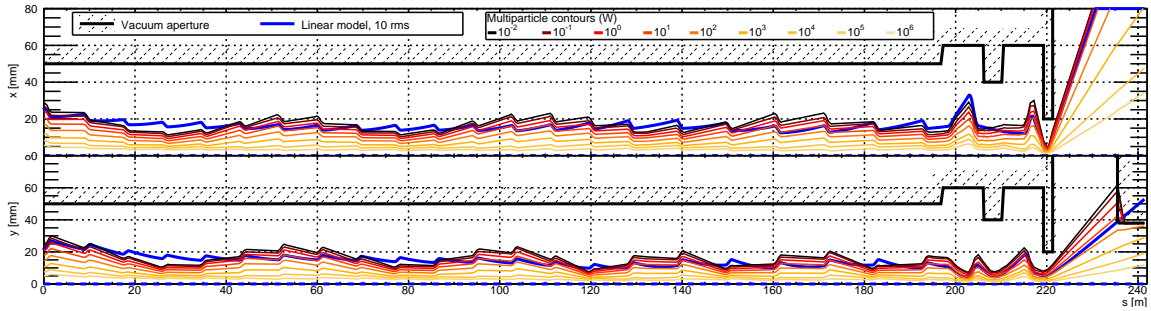| Element	Parameter	Unit	Static	Dynamic
Quadrupole	dx, dy	mm	0.2	0.01
	$d\hat{z}$	deg	0.03	0.003
	Gradient	%	0.5	0.02
Dipole	dx, dy	mm	0.2	0.01
	$d\hat{z}$	deg	0.03	0.003
	Strength	%	—	0.02
Beam	dx, dy	mm	2	0.25
	dx', dy'	mrad	0.1	0.01
	Energy	MeV	20	2.5
	Emittance	%	10	1
	Mismatch	%	10	1
	Current	mA	1	0.1

Figure 2: Multiparticle simulations including dynamic and corrected static errors.

Low intensity losses (on average 11 W, max. 100 W) are observed at the target monolith edge ($s \simeq 236$ m) with typically 0.6 kW, max. 1.4 kW, hitting the inner walls of the monolith beam duct leading to the target [6]. The loss magnitudes are not considered critical, and it should be noted that this can be reduced by adjusting the beamlet dimensions. It should be noted that the simulated primary beam losses can depend very much on the input distribution. A complementary statistical study of the end-to-end ESS accelerator and transport line to the target has been conducted [8] and this revealed a far smaller degree of losses near the target.

It is very comforting to see that the simulations indicate that the beam waist at the Neutron Shield Wall (NSW) aperture ($s \simeq 220$ m) can be preserved despite applying the errors. Similarly, the simulations indicate a substantial normalized aperture at the location of the RSMs ($s \simeq 207$ m), despite their reduced physical aperture, cf. also [5].

3.2.2 RSM Harmonic Content

A systematic sextupole contamination is expected to scale with the nominal AC dipole field. To evaluate the sensitivity towards this, a sextupole field was introduced in all RSMs with a strength of $u_3 = \int \Delta B dL / \int B_0 dL$ units (10^{-4} of the dipole field) at the specified good field radius of ± 15 mm (for reference, the inner aperture radius is specified
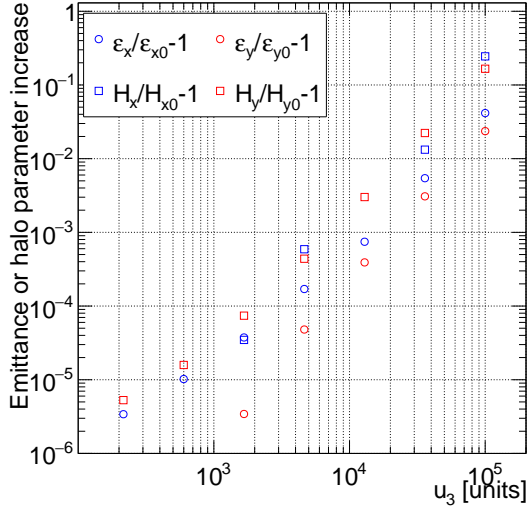
Figure 3: Emittance and halo increase as a function of the level of sextupole contamination.
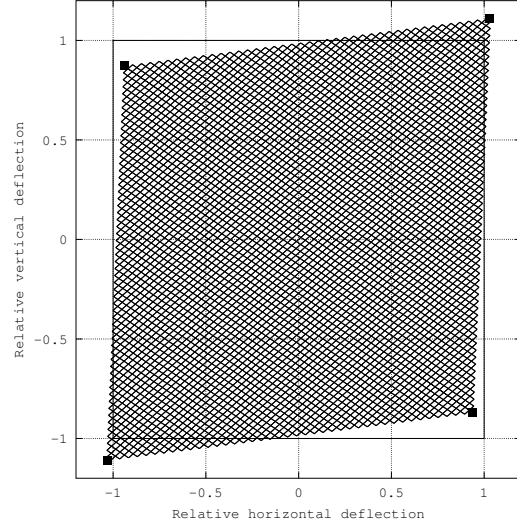

Figure 4: RSM roll errors. The outline of the relative Lissajous-pattern is distorted according to the average values of the roll errors.

to 40 mm). For a number of values of u_3, a multiparticle simulation is performed based on 10^6 particles being tracked through the raster section and to the target. We consider a snapshot where the raster displacement is at maximum H amplitude and zero in the V direction, *i.e.* the sextupole contamination only originates from the H raster magnets. In each case, the resulting growth of RMS emittance and halo parameters was calculated for the unrastered beamlet at the target, and the result can be seen in Fig. 3. The relative changes tend to follow a power law within the used multipole contamination range. Due to the small beam size and displacement along the raster section, the beam is quite insensitive to even considerable sextupole strengths. The beam effects do not reach the level of $\lesssim 10^{-3}$ when $u_3 \lesssim 10^4$. Additionally, the raster pattern is expected to smear modest differences in emittance and halo of the beamlet. Considering potential late changes in the beam dimensions along the raster magnet section, the specifications are conservatively set to $u_3 < 10^3$ or $< 10\%$ field deviation per magnet at the good field radius, which should be easily attainable from a magnet designer's point of view.

3.2.3 RSM Alignment

Inherently, a dipole is somewhat insensitive towards transverse alignment errors. Considering also the resulting beam's tolerance towards higher harmonics, cf. section above, the requirements for transverse alignment is relatively modest. On the contrary, static RSM roll errors will be directly visible in the distribution produced at the target. The net effect will predominantly be a shearing of the pattern outline. Whereas the relative raster pattern is ideally square with corners located in $\pm(1, \pm1)$, small roll errors will effectively shear the pattern into a parallelogram with its corners in $\pm(\cos(\langle \hat{z}_x \rangle) \mp \sin(\langle \hat{z}_y \rangle), \cos(\langle \hat{z}_y \rangle) + \sin(\langle \hat{z}_x \rangle))$ where $\langle \hat{z}_x \rangle$ and $\langle \hat{z}_y \rangle$ are the average roll errors in the horizontal and vertical raster magnet sets, respectively. Additionally, even a roll distribution with zero average, but large variance, will reduce the relative pattern amplitudes without otherwise distorting the pattern.

8

To demonstrate the effects of roll errors, a pattern resulting from 8 RSMs with roll errors sampled from a considerably wide uniform distribution of $|\hat{z}| < 100$ mrad has been simulated and can be seen in Fig. 4. The roll alignment of each RSM is believed to be possible to a level of better than $|\hat{z}| < 1$ mrad, *i.e.* thus only leading to minuscule effects.

3.3 Waveform

The magnetic field waveforms produced by the RSMs will contain distortions and other effects that arise in a realistic system of components with finite parameters.

3.3.1 Waveform Bandwidth

Imperfect synchronization will degrade the pattern and the resulting beam distribution. There are three levels of synchronization that need to be addressed to ensure proper performance: within each raster modulator (*e.g.* the switches in H bridge, cf. Sec. 4), magnet-to-magnet synchronization in a set, and finally maintaining the frequency ratio and phase ϕ_{xy} between the two transverse directions. The first two sources will contribute to the upper cutoff frequency of the waveforms, whereas the latter could affect the generated pattern directly.

The raster system should apply triangle field waveforms, defined by an infinite sum of odd harmonics, with a corresponding ideal square waveform sweep velocity. Finite bandwidth of the raster system will however truncate the waveforms, leading to finite rise and fall times (t_r) of the sweep velocity waveform. To evaluate the necessary upper 3 dB cutoff frequency of the system ($f_{c,2}$), we compare the velocity waveform rise time $t_r \simeq 0.350/f_{c,2}$ with the time to sweep the beamlet 3 RMS sizes, $t_{3\sigma} = 3\sigma_w/4a_w f_w \simeq 1.9\ \mu$s, assuming the constant sweep speed far from the transition

$$\frac{t_{3\sigma}}{t_r} = \frac{f_{c,2}}{0.350} \frac{3\sigma_w}{4a_w f_w} = \frac{15}{7} \frac{\sigma_w}{a_w} \frac{f_{c,2}}{f_w} \ .$$

Ideally, $t_{3\sigma}/t_r \gg 1$, resulting in edges with an intensity not significantly larger than in the center of the distribution. The relative beamlet size thus compensates for a finite bandwidth of the raster system. Since $\sigma_w/a_w \gtrsim 0.1$, $f_{c,2} \gtrsim 5f_w = 200$ kHz is found. In Fig. 5, the raster pattern and target intensity distribution is simulated for three values of $f_{c,2}$. It should be noted that the filtering also reduces the waveform amplitude (noticeable in the upper panels). This effect has been compensated for in the simulation of the intensity distributions, hence the seeming improvement in peak current density when $f_{c,2}$ is reduced. The distribution for $f_{c,2} = 200$ kHz appears quite acceptable, whereas $f_{c,2} = 100$ kHz contains artefacts, vertical ridges and corner peaks. The bandwidth requirement is set at 200 kHz (or the fifth harmonic of the maximum raster frequency to be used).

3.3.2 Waveform Amplitude Stability

Due to the scheme of producing the triangle waveforms, any temporal jitter in *e.g.* the reference clock will directly translate into amplitude jitter. The raster waveform amplitude stability over several raster pulses is modeled as a Gaussian distribution with RMS $\sigma_{p-p}(a)$. It is important to bear in mind that the beam RMS size is considerable compared to the nominal raster amplitudes, $\gtrsim 20\%$. Even with nominal parameters the time-averaged beam distribution, resulting from a convolution of the two distributions, differs

(a) $f_{c,2} = 100$ kHz   **(b)** $f_{c,2} = 200$ kHz   **(c)** $f_{c,2} = 300$ kHz
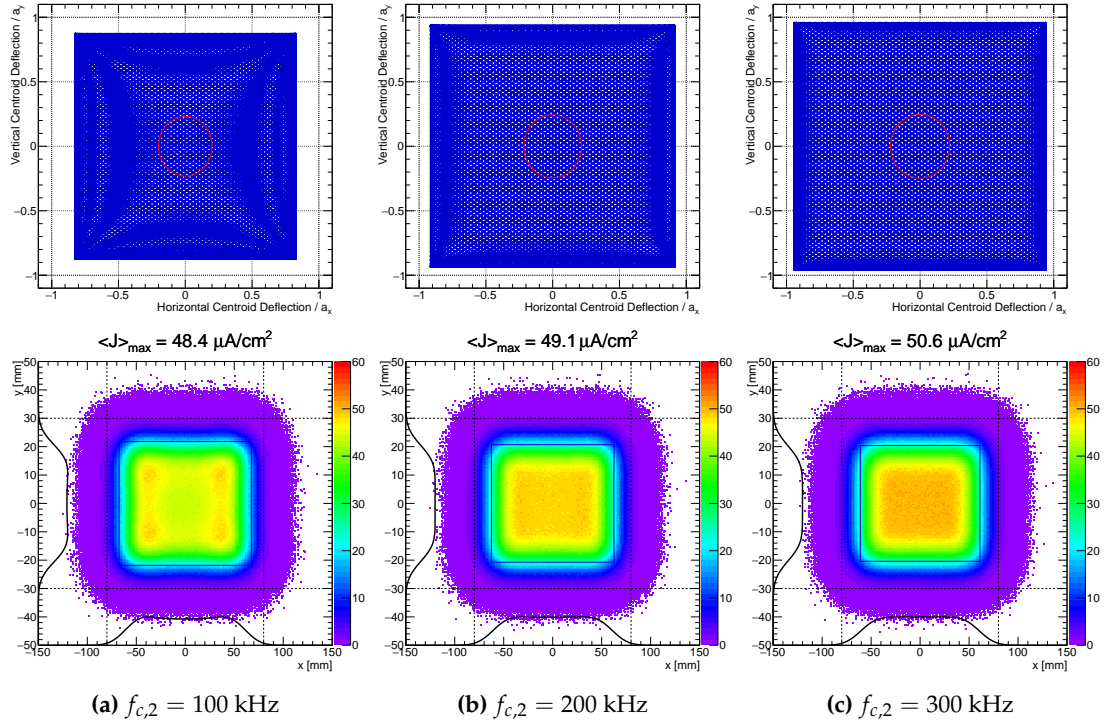
Figure 5: Raster pattern and intensity distribution on the target (BEW) based on waveforms that have been subjected to 1st order Butterworth filter with a cutoff frequency $f_{c,2}$.

already considerably from an ideal tophat distribution, cf. red curve in Fig. 6. If the produced waveforms should vary in amplitude of the order of *e.g.* $\sigma_{p-p}(a) \lesssim 1\%$, it should be expected to not change the delivered beam to a noticeable extent, cf. blue curve in Fig. 6.

In conclusion, the raster system has been shown to provide a very flat beam distribution to the target and PBW, while being relatively insensitive to alignment and beam parameter errors.

4 BDS Engineering Design

The total raster system is foreseen to consist of $n_{\mathrm{RSM}} = 8$ subsystems: 8 colinear raster scanning magnets (RSMs), two sets of 4 acting in the respective transverse planes. The RSMs in a set should ideally be synchronized and share the same field amplitude. The same RSM and modulator design is applicable to both the horizontal and vertical set of RSMs, differing only by magnet orientation. The RSMs are placed in pairs of identical field direction, $(B_y B_y)(B_x B_x)|BI|(B_x B_x)(B_y B_y)$. A RSM pair shares a single 850 mm ceramic vacuum tube with metallic flange connections, and the first half of the raster system is shown in the lower panel of Fig. 7[1]. At the centre of the RSM section, a beam instrumentation (BI) unit is placed. This unit is not a part of WP6's responsibility. The interfaces between the RSM equipment and the BI unit are spatial (slot sizes), connecting flange types, and stray fields from the RSMs.

Each RSM is powered by a dedicated modulator. Not only does this modular design

---

[1]A better and more technical drawing is included later in this report, cf. Fig. 9.
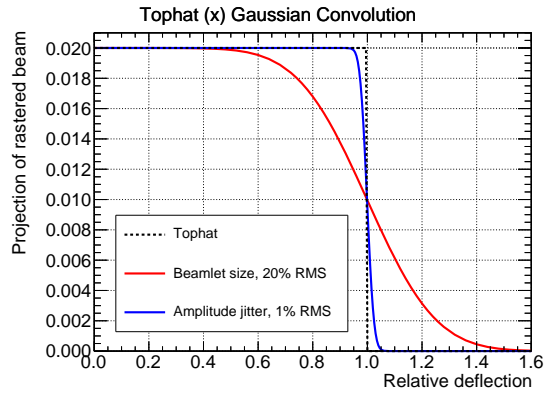
10

Figure 6: Convolution of an ideal tophat with Gaussian distributions having different RMS values.
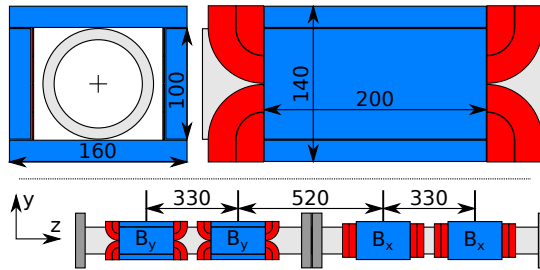

Figure 7: Early sketch of dimensions of a raster magnet (top panel) and the positioning of RSM pairs introducing orthogonal field components (bottom panel). Ferrite parts are shown in blue and copper coils are shown in red. An outer frame to hold the yoke pieces together is not shown here.

reduce the magnetic load on the RSMs and the peak output power of each modulator, but it is also a straightforward approach to implement redundancy and in general reduce the impact of element failures. The total system is specified to be able to deliver nominal operation, despite a single permanent RSM or modulator failure in each set. The remaining 3 RSM subsystems (RSM + modulator) in the set can then be adjusted to compensate with 33% amplitude increase. Each subsystem thus provides a notable contingency in the available peak bending strength, cf. Table 3. Similarly, an increased beam rigidity, in case of linac upgrades, can be compensated by simply adding more raster units.

To avoid the need for active cooling of magnets and power supplies, the raster system is foreseen to be operated at a duty cycle of only 5%, appropriately more than the 4% beam pulse duty cycle, 2.86 ms at 14 Hz. While the raster pulse duration is a configurable parameter, the repetition rate is dictated by a pretrigger that precedes the beam pulses.

As mentioned previously, a major part of the conceptual design was performed in collaboration with the group for fast pulsed (magnet) systems at CERN and later Danfysik. The outcome is described in [9] and [1], with the latter one being more detailed. Among other topics, 3D magnetic field calculations, choice of materials and cables, and power supply topology and regulation were considered here. A cross section and side view of a horizontal RSM (*i.e.* with a vertical field component) can be seen in Fig. 7. The magnet is based on a window frame yoke that gives good field uniformity in a large region of the magnet aperture. To avoid burn-in near pattern edges and corners, the sweep speeds should ideally be constant, while the direction alternates as dictated by the frequency.

11

Table 3: Top level parameters and specifications of a RSM.

Parameter	Unit	Value
Beam rigidity	T.m	9.29
Beam pulse (4%)	ms	2.86
Raster pulse (5%)	ms	3.57
Max. f_w	kHz	40
Waveform	—	Triangle
Min. magnet aperture	mm	100
Magnetic length	mm	300
Turns per coil	—	2
Peak strength	mT.m	5
Nom. strength (H / V)	mT.m	1.6 / 2.3
Nom. deflection (H / V)	mrad	0.17 / 0.25
Max. current (peak-to-peak)	A	±340
Max. voltage (peak-to-peak)	V	±650

The magnet field should thus follow a triangle waveform. The considerable operating frequency—including the harmonics necessary for the triangle waveform—calls for materials with low eddy current losses and a high frequency response. A NiZn ferrite yoke, possibly CMD5005 from Ceramic Magnetics, would be an obvious choice. Due to the skin depth in Cu, $\delta = 0.3$ mm $\times \sqrt{40\,\text{kHz}/f_w}$, the magnet coils will not benefit from bulk volume being more than $\simeq 0.5$ mm from the coil surface. The conductors are thus cut from a 1 mm thick OFHC Cu plate and bent into 2-turn bedstead coils, cf. Fig. 7.

Each RSM will feature a Bdot loop, which typically consists of a single wire winding around the magnet yoke or pole (not applicable in the current RSM design). A current that is proportional to the rate of change in magnetic flux through the loop will be induced, hence the name. For an ideal triangle field waveform, the Bdot waveform is thus a square waveform. Additionally, each supply could contain Idot loops (a current transformer) that measures the rate of change in cable current, *i.e.* ideally also a square waveform. Both signals can be used to verify the magnetic field, as has been done in other raster magnet applications [10]. The Bdot and Idot signals are considered complementary, although the Bdot relates more directly to the produced magnet field waveforms, *i.e.* includes potential temperature-dependant changes in magnet inductance.

4.1 Cable Options

A considerable cable length of 30 m is specified between the RSMs and their associated power supplies, since the former are located in the A2T tunnel and the latter are located in the Gallery Support Area (GSA). Special cable types must thus be considered to not reach excessive cable inductance values. With the required fundamental raster frequencies of 40 kHz, attention should be payed to the typical AC effects in conductors, the skin effect and proximity effect. In [1], three cable types are considered:

Litz wire consists of a braid of numerous insulated wires. Designed to reduce skin and proximity effects up to the MHz range. To obtain longer lengths of Litz wire or connect several wires in series is believed to be difficult.

Coaxial cable for high currents is expensive and is, due to its larger diameter, difficult to bend, which may introduce installation complications.

4-Core wires provides four conductors that are arranged in a quadrupole layout and thus minimizes the cable inductance. The cable type are available from several manufacturers. The cable type allows for simple interconnections and relatively short radii of curvature.

Results of electrical circuit simulations of the components of a modulator and the electrical equivalent of a RSM were also provided [1]. The simulations assumed two 4-core wire cables (Draka FXQJ-CU EMC-35 mm^2 or equivalent) and exhibited more than acceptable waveform performance. Due to this and the advantages listed above, this cable type is chosen for the design.

4.2 Ceramic Chamber Metallization

With the required magnitudes of dB/dt, a ceramic vacuum chamber is required. In various accelerator applications of longer ceramic vacuum chambers, the inner surface is required to be metalized. An inner $\simeq 1 \, \mu$m Ti metallization layer can thus be applied to:

- avoid build-up of beam-induced charges along the ceramic. These could potentially mis-steer the beam or lead to strong discharges. The metallization would allow the beam-induced charges to be constantly drained from the inner walls.

- conduct the beam image currents and avoid heating of the ferrite yoke. If not mitigated, the ferrite could be heated to near or above the material's Curie temperature, where a phase transition occurs that changes the material's magnetic properties. The metallization would screen the ferrite yoke against wake fields.

When applied, care should be taken to the thickness of the metallization [11, 12], such that it does not distort the field waveform in terms of a delay and bandwidth (amplitude and sharpness of peak) reduction. It is worth stressing that introducing a constant delay in field is not considered critical if similar in all magnets, whereas attenuation of the field amplitude will have to be compensated by increasing the modulator amplitude setpoint. Although the ESS beam and raster waveform frequencies are several orders of magnitudes apart, it can be technically difficult to achieve the proper thickness of the metallization.

Regarding the build-up of beam-induced charges, the effects are not believed to be relevant for the rigid beam that is expected in the high-energy part of the ESS accelerator.

Storage rings, which typically operate at beam currents two orders of magnitude larger than the ESS, typically feature ferrite-based kickers *including* a beam screen. On the other hand, boosters and other low-current accelerators can usually make do with in-vacuum ferrite kickers that are unshielded from the beam wake fields and typically rather close to the circulating beam.

Following this reasoning, the ceramic beam tubes of the ESS raster system are *not* to be internally metallized in the baseline design. Accelerator community experts have been contacted to support this decision, and the final decision should be taken before the supplier's detailed design is completed. The supplier is also to comment on whether this is appropriate given the expected range of beam parameters and precedence with similar equipment. Once the pre-series are constructed, the long-term beam-induced heating of the ferrite pieces could possibly be tested by suspending a (movable) wire through the magnets. As used in BPM test stands, a waveform generator would introduce a suitable current in the wire to mimic the beam.

4.3 ICS

A conceptual block diagram of the modulator can be found in [1, Sec. 4.6]. In brief, the modulator consists of:

- Local control electronics based on a microprocessor (μP).

- Input converter: a DC capacitor charging supply.

- Output converter: an H bridge to modulate the DC link voltage into a square voltage waveform across the magnet.

- Feedback and regulation controller.

The supplies shall be able to operate in local and remote mode. In local mode, the supply shall be controllable through the front panel. Control and monitoring of the supply in remote mode shall be made via Ethernet and TCP/IP. A complementary block diagram can be seen in Fig. 8. Contrary to the former, this diagram also illustrates how the raster system is foreseen to relate to interfacing systems, such as the Integrated Control System (ICS) and Machine Protection System (MPS). The ESS timing event receivers broadcast the current accelerator operational mode (*e.g.* beam energy). This information shall be used to configure the raster supplies. The timing event receivers will also generate a high-frequency (88 MHz) timing signal that is to be used as input for the power supplies. The raster supplies shall generate waveforms that are based on these timing signals. We expect that this equipment lies within the responsibility of the ESS ICS group. Additionally, we expect that the group will deliver and configure this hardware for off-site testing, *e.g.* the pre-series long-term performance acceptance test at AU. We believe that this test will be even more valuable, if the pre-series setup is tested with the interfacing equipment that is to be used at ESS.

4.3.1 MPS

As illustrated in Fig. 8, each individual RSM modulator will commence the raster pulse relative to a pretrigger from an ESS timing event receiver. The modulator will verify that the raster pulse is apparently correct in terms of raster waveform parameters and timing relative to the configuration and timing. An OK/NOK signal ("RSM Power Supply (PSU) Status") shall be stated and delivered to a dedicated Fault Detection Unit (FDU), which interfaces directly with the ESS Beam Interlock System (BIS), cf. Fig. 8. Besides this, the unit will receive Bdot (and possibly Idot) waveforms from each RSM modulator through an isolated output (0–10 V). The FDU will digitize and perform analysis of the sum of waveforms from each RSM set (H or V), *i.e.* what the beam is subjected to (if the beam's time to transit the colinear set of magnets is neglected). From such sum-waveforms, synchronization errors and other issues can easily be detected.

As indicated in Fig. 8, the FDU is not the responsibility of AU. The FDU will be developed by ESS ICS under the responsibility of Annika Nordt, possibly in collaboration with consultants from Zürcher Hochschule für Angewandte Wissenschaften (ZHAW). Already now, the functions of the RSM system is being reviewed by AU with the help of these experts. The aim of this study is to provide suggestions that can assist and guide the final design in terms of reliability.

The reference [13] contains further details on protection in this region and detection of errant beam conditions. Although designed at a different time, [10] contains information about the protection concepts in a similar raster system.

4.4 RAMI

Only a few comments can be given at this stage as the Reliability, Availability, Maintainability and Inspectability (RAMI) procedures will be developed together with the vendor during the design phase. Some experience will exist by the vendor, who is required to have previous experience. Whether we will be able to provide quantitative predictions is at this stage unknown. It is commonly known that bottom-up approaches to assessing the reliability of complex systems often yield numbers that can be orders of magnitude off due to manufacturing details. Some experience will be obtained during the long-term tests (many months) at Aarhus University, where failures will be logged and analysed on two magnet+modulator units. As already described, the production-series RSM system will consist of:

1. a power supply (input converter, output converter and control electronics).

2. a magnet (window-frame ferrite with ceramic vacuum chamber and two air-cooled, thin, flat 2-turn copper plate coils.

3. two 30 m power cable connecting the above, located in the GSA and A2T tunnel, respectively.

4. support stands with alignment capabilities.

8 such units will be installed and used under normal operating conditions. Hence the complete RSM system will consist of 4H+4V highly independent systems, which provide full nominal operation. In case of *e.g.* the permanent failure of a single RSM power supply, operation can be continued with only 7 RSMs, 3H+4V or 4H+3V, by only readjusting the strengths of the remaining 3 RSMs in the affected set. The system will thus provide a high degree of inherent redundancy.

4.4.1 Random Failures

The expected most frequent failure will be a failing single power supply unit, and a spare power supply unit should be available for easy exchange (a matter of hours) at the next shutdown as the complete system can operate with one failing unit in each plane. Cables and magnets are expected to fail at a much lower rate (in particular if preventive maintenance and regular inspection is carried out). Nevertheless, we suggest that one spare magnet should be provided.

4.4.2 Lifetime issues

With relatively rugged magnets built from radiation resistant materials, the lifetime of the components are expected to be years. Clearly, attention will have to be paid to radiation resistance when making material choices for the system, *e.g.* cable insulation.

As the components are relatively small and the system is inherently redundant, operation can be resumed after a few minutes for the most common failures. Since no water-cooling is needed in neither the magnets, supplies, nor the vacuum system, only vacuum leaks would require a replacement lasting more than a few hours. The power supplies are installed in the more remote GSA, where radiation levels are expected to be low, and a failing supply can be replaced within less than one hour, if the personnel are trained for the procedure.

4.4.3 Catastrophic Events

Events like vacuum leaks, fire and the like can be mitigated by detection and interlocks and subsequent accelerator shutdown. Secondly, having spare hardware available for replacements will reduce the amount of unscheduled downtime.

4.5 Safety

Again, these issues have only been touched upon in a rudimentary way, as they will be developed together with the supplier of the system.

4.5.1 Conventional Hazards

The hazards will involve high voltage (below 1000 V), mitigated by ordinary shielding and warning signs. Any high voltage (greater than 50 V DC) shall be shielded. A basic separation between power and signal cables shall be provided. Each magnet shall have its coils connected internally on the magnet with only two terminals (+ and -) on each magnet for connections of the external power leads. Enclosure covers shall be removable only with use of tools. Cables and feed-throughs will be similarly protected as is normal practice. Mechanical hazards, heavy weights will also follow ordinary practice.

4.5.2 Radiation Hazards regarding Gamma Blockers

Gamma Blockers (GBs) are potentially needed both in the A2T and the Dump Line. Briefly put, a GB inserts a shielding plate into the beam pipe, thus blocking line of sight to areas that have been severely activated by the beam. Typically, the electromagnetic part of the backshine can be effectively stopped by a shield with a thickness corresponding to several radiation lengths. This can thus significantly reduce the upstream residual dose rates before a maintenance crew is to access the tunnel. To evaluate the need for and specifications of the GBs, extensive simulations of the backshine are to be performed. To conduct such studies is quite beyond the expertise of AU. Simulations of the target backshine have however been carried out by the University of Huddersfield, ESS, and National Centre for Nuclear Research (NCBJ) in Swierk. Initial design and calculations of the GBs are presently being performed by the latter. Levels of the order of tens of mSv/h after 1 hour of cool-down are believed to necessitate the use of a thick ($\simeq$ 200 mm) plate of a dense material like steel (or maybe even W or Pb). Currently, the studies are following the design of the similar unit at SNS. Conclusions will be provided by a report to be delivered in November by the Swierk group. Swierk is subsequently supposed to build the GBs for both the A2T and the Dump Line. Heads-of-Agreement between Swierk and ESS is presently being negotiated.

5 CAD Models

Based on the A2T lattice and the RSM dimensions suggested in [1], an engineer at Aarhus University has drafted a CAD model of the magnets, vacuum chambers and bellows, magnet support & alignment, cf. Fig. 9. The model has been distributed for comments from various technical groups and disciplines at the ESS. Among other parts, the vacuum design was improved vastly following constructive comments (number and location of bellows, flange types, support design, *etc.*).

It should be noted that the CAD drawing does not necessarily represent the final design, but should act as a strong inspiration for the future supplier. The CAD model has been uploaded to the ESS model database and kept up to date here.

6 Procurement of the RSM

As it maybe appears from the above, our plan is not to develop and describe the RSM system to its full detail with only production to follow. Instead, we have during the design phase developed the technical details, together with a potential supplier of the system, to the extent that proved the feasibility of the system. The details will be used, slightly modified, in the call for tenders. When a supplier has been chosen, the very detailed design will subsequently be developed by the supplier and AU. Before any major production phase is initiated, the supplier's suggestions and plans are to be approved by AU and the ESS. For example, we expect that experts at ESS will also verify the supplier's detailed design before the pre-series is put into production. We believe that it is important that ESS is engaged with (at least) some (minimum) involvement at these stages. Ideally, a minor CDR would be held at the more critical stages.

6.1 Procurement Material & Specifications

Belonging to a university in Denmark, ordinary procurement rules has to be followed, and it is our plan to go out for a call for tenders immediately following the CDR. The tender documents [3, 2] have been written with an appendix containing the technical specifications [4]. As it appears from Sec. 4, a potential vendor has together with us developed a RSM system in some detail [1]; clearly this vendor is a potential candidate to build the actual system. However, the already developed results and descriptions of the RSM system, the resulting note [1], will openly be made part of the tender material. We note here that the technical specifications have been updated since the final version of the note, and the technical specifications of the tender material [4] should be considered the single point of truth in this respect.

In Sec. 1.1, it is described how the major phases following the procurement are anticipated to take place. More information on the schedule can be found in [2, Sec. 3]. Information about expected Factory Acceptance Test (FAT) and Site Acceptance Test (SAT) procedures is found in [4, Sec. 3].

6.2 Quality

The requirements to the selected vendor will include a minimum turnover together with recent production of similar turnkey pulsed magnet systems and ISO 9000 conformity, cf. Section 5.3–5.4 of [2].

7 Verification Planning

Part of the procurement and subsequent contract will include a FAT before any material (pre- or production-series) is shipped from the supplier. Furthermore the plan to install the production-series at ESS, assumed to involve staff from Aarhus University, will also

include some Site Acceptance Test (SAT). Preceding this will be long-term pre-series testing, as mentioned above. Section 3 of [4] contains further details regarding the planned verification steps.

8 Acronyms

AU   Aarhus University

A2T   Accelerator to Target

BDS   Beam Delivery System

BEW   Beam Entrance Window

BIS   Beam Interlock System

CDR   Critical Design Review

CO   Crossover

ESS   European Spallation Source

FAT   Factory Acceptance Test

FDU   Fault Detection Unit

GB   Gamma Blocker

GSA   Gallery Support Area

HEBT   High Energy Beam Transport

ICS   Integrated Control System

IVDR   Internal Vertical Design Review

MPS   Machine Protection System

NCBJ   National Centre for Nuclear Research

NSW   Neutron Shield Wall

PBW   Proton Beam Window

PSU   Power Supply

RAMI   Reliability, Availability, Maintainability and Inspectability

RSM   Raster Scanning Magnet

SAT   Site Acceptance Test

WP6   Work Package 6

ZHAW   Zürcher Hochschule für Angewandte Wissenschaften

References

[1] Danfysik, H. D. Thomsen, and S. P. Møller, "Conceptual design of raster scanning system," tech. rep., ESS, 2014.

[2] H. D. Thomsen and S. P. Møller, "Instructions to tenderers." RSM Tender Material, September 2015.

[3] H. D. Thomsen and S. P. Møller, "Contract." RSM Tender Material, September 2015.

[4] H. D. Thomsen and S. P. Møller, "Appendix 1: Technical Specifications." RSM Tender Material, September 2015.

[5] H. D. Thomsen and S. P. Møller, "The ESS High Energy Beam Transport After the 2013 Design Update," in *WEPRO073*, 2014.

[6] H. D. Thomsen and S. P. Møller, "Performance of the ESS High Energy Beam Transport under Non-nominal Conditions," in *IPAC'14 Dresden, Germany*, no. WEPRO074, 2014.

[7] R. D. Duperrier *et al.*, "CEA Saclay codes review for high intensities linacs computations," in *ICCS'02*, no. LNCS 2331, p. 411, 2002.

[8] M. Eshraqi, R. de Prisco, R. Miyamoto, E. Sargsyan, and H. D. Thomsen, "Statistical Error Studies in the ESS Linac," in *IPAC'14 Dresden, Germany*, 2014.

[9] H. D. Thomsen and S. P. Møller, "The Design of the Fast Raster System for the ESS," in *IPAC'14 Dresden, Germany*, no. WEPRO072, 2014.

[10] R. Sheffield and M. E. Schulze, "Raster Magnet System for Expanding the APT Proton Beam," Tech. Rep. LA-UR-99-5820, Los Alamos National Laboratory, 1999.

[11] M. Barnes, T. Fowler, M. Atanasov, T. Kramer, and T. Stadlbauer, "Effect of a Metallized Chamber upon the Field Response of a Kicker Magnet: Simulation Results and Analytical Calculations," in *IPAC'12 New Orleans, USA*, no. THPPD074, 2012.

[12] Z. Lazic and C. Martins, "Modelling of uhv pipe copper coating influence on the magnetic field of the raster magnet," tech. rep., ESS, August 2013.

[13] T. Shea, L. Coney, R. Linander, A. Jansson, E. Pitcher, A. Nordt, C. Thomas, and H. D. Thomsen, "Instrumentation and machine protection strategy for the ESS target station," in *ICANS*, no. ABT-08, 2015.
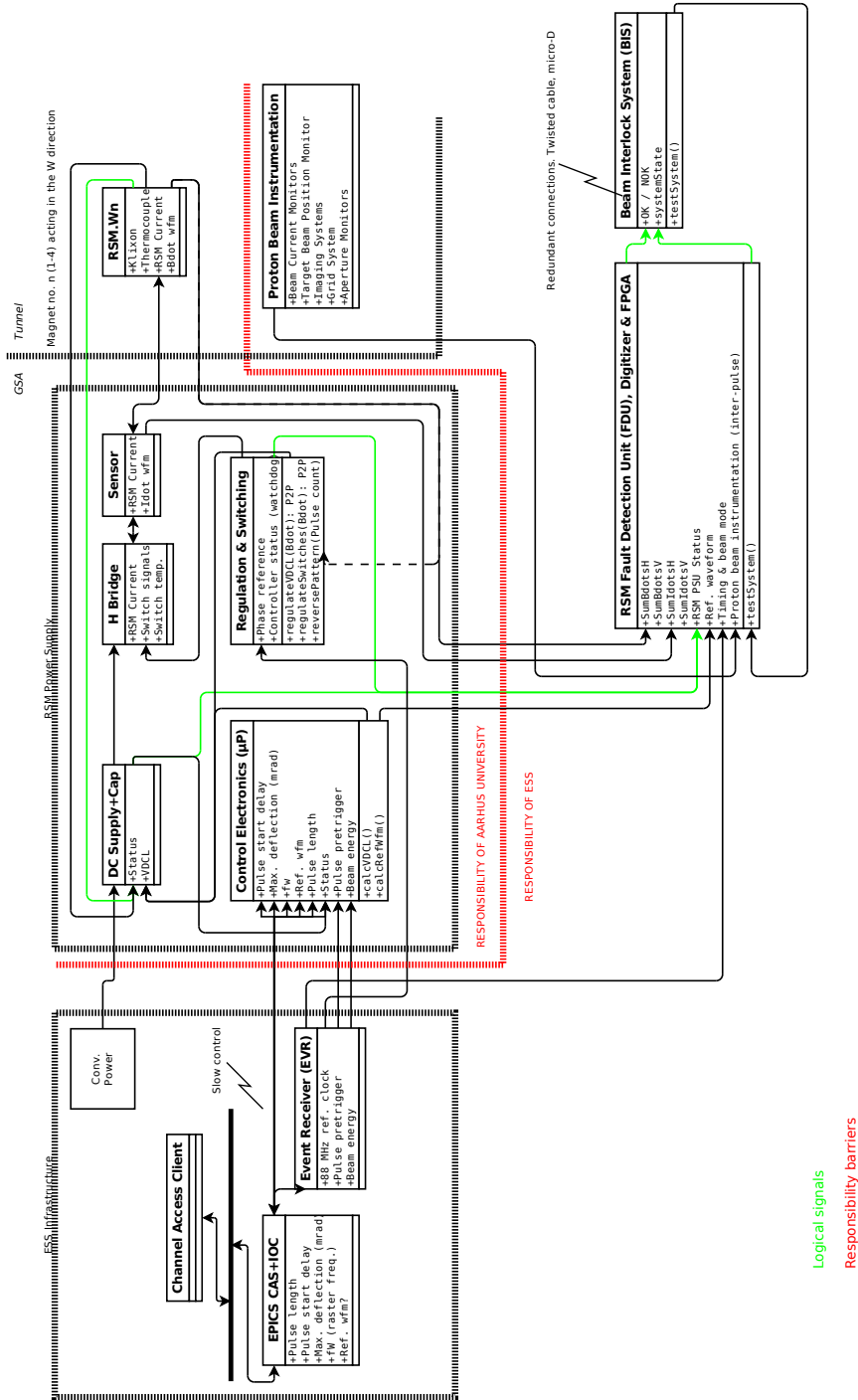
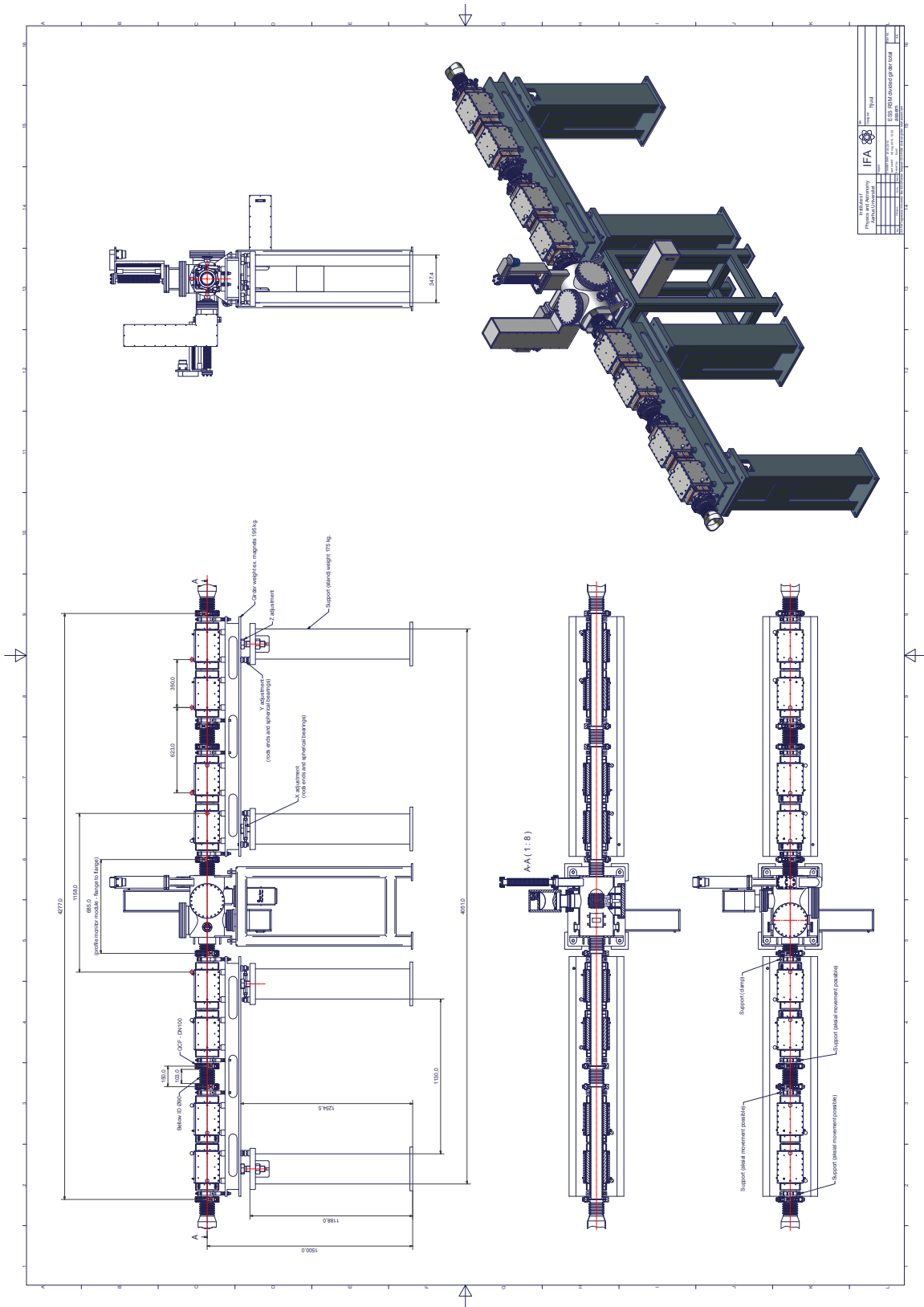Figure 8: A block diagram of a single RSM and its power supply / modulator.

Figure 9: CAD model of the 8 raster magnets distributed across two girder-based support stands.